Stoichiometry control in molecular beam epitaxy of $BaSnO_3$

Nicholas G. Combs, Wangzhou Wu, and Susanne Stemmer*

Materials Department, University of California, Santa Barbara, CA 93106, USA

* Corresponding author; email: stemmer@mrl.ucsb.edu

Abstract

La-doped $BaSnO_3$ films were grown on $DyScO_3$ substrates by molecular beam epitaxy using La, Ba, and SnO_2 sources with and without additional oxidant, respectively. Lattice parameter measurements as a function of growth conditions show a reduced lattice parameter that is likely due to substitution of Sn^{2+} on the Ba-site. The propensity for the antisite defect is discussed as being due to the combination of oxygen-poor, Sn-rich conditions and the dual valence of Sn. Although electron mobilities are highest for films with reduced lattice parameters, anti-site defects will pose an upper limit to thin film mobility. Less Sn-rich conditions lead to the formation of another defect that causes a lattice expansion. The combined effects of these defects on the lattice parameter can compensate each other and cause the appearance of a stoichiometric lattice parameter for nonstoichiometric films with poor electrical behavior.

I. Introduction

The cubic perovskite $BaSnO_3$ has gained significant interest for applications as a transparent conducting oxide and as a candidate material for next-generation high-frequency and high-power electronics applications [1-6]. Its promise for these applications stems from the combination of a relatively wide bandgap (~3 eV) [1-3, 7-9], low effective conduction band mass [10], high electron mobility at high carrier densities [1-3], and epitaxial integration with other perovskite oxides [5]. La-doped $BaSnO_3$ single crystals exhibit room temperature electron mobilities as high as 320 $cm^2V^{-1}s^{-1}$ at a doping density of 8×10^{18} cm^{-3}, a record among perovskite oxides [1, 2].

Epitaxial thin films are needed for devices, but have yet to reach single crystal mobilities. Low carrier densities have also been difficult to achieve, a clear indication of the presence of compensating defects. To-date, the highest mobility films are grown via molecular beam epitaxy (MBE) using a SnO_2 effusion cell as Sn (and oxygen) source. These films show Hall mobility values around 150 $cm^2V^{-1}s^{-1}$ to 180 $cm^2V^{-1}s^{-1}$ [11, 12]. The use of the SnO_2 source proved crucial for high-mobility films [11]. It addresses a key challenge in the MBE of stannates, namely that Sn reacts with co-supplied oxygen to form volatile SnO, leaving unoxidized Sn behind [13, 14]. The difficulty in oxidizing Sn in MBE conditions is the likely culprit for the lower mobilities of $BaSnO_3$ films grown using a metallic Sn source [15] or metal-organic Sn precursor [16, 17].

Ultimately, one of the most significant hindrances to high mobilities will be the high density of threading dislocations that are typical for epitaxial films grown on highly mismatched substrates. The relatively large lattice constant of $BaSnO_3$ (~ 4.117 - 4.115 Å [8, 18, 19]) results in a significant lattice mismatch with commercially available perovskite substrates such as

$SrTiO_3$ (-5.1%) and $DyScO_3$ (-4.2%). Nevertheless, a large variation in mobility values is observed even for films grown on identical substrates under similar conditions. Furthermore, mobilities on different substrates do not scale with lattice mismatch, even though the threading dislocation densities roughly do [11, 12]. These findings indicate that $BaSnO_3$ films contain high concentrations of point defects, most likely arising from nonstoichiometry, that negatively impact thin film mobilities. While adsorption-controlled growth [12, 17] ensures the formation of the $BaSnO_3$ perovskite phase, there is as yet no evidence that these films are perfectly stoichiometric.

The dual valence state of Sn is one of the main challenges in MBE of stoichiometric $BaSnO_3$. While Sn^{4+} is favored in oxidizing conditions, reducing conditions promote Sn^{2+} [20]. As a result, II-IV perovskites such as $BaSnO_3$, where the cations take on formal charges $A^{2+}B^{4+}O_3$, may allow Sn to occupy both the A- and B-sites [21]. Consistent with this possibility, density functional theory (DFT) calculations show that the antisite defect, Sn_{Ba}, is a low-energy defect in $BaSnO_3$ in oxygen-poor conditions [22].

The goal of this study was to develop an improved understanding of the challenges in growing stoichiometric $BaSnO_3$ films in MBE from a SnO_2 source. To this end, we grew films both with and without the presence of an additional oxidant. The fact that perovskite $BaSnO_3$ can be grown without any additional oxygen shows that the SnO_2 source supplies not only Sn but is also the main source of oxygen in $BaSnO_3$ MBE. Lattice constants of almost all films were lower than the stoichiometric value, and it is posited that a significant amount of Sn_{Ba} anti-site defects are the cause. Shifts in the growth parameters when oxidants co-supplied provide additional insights into the challenges in stoichiometry control.

II. Experimental

La-doped $BaSnO_3$ films were grown by MBE on (110) $DyScO_3$ substrates. High-purity Ba, SnO_2, and La-dopant were co-evaporated from separate effusion cells, as described elsewhere [11]. Ba and SnO_2 fluxes were calibrated using an ion gauge placed at the position of the substrate and are given as beam equivalent pressure (BEP). Prior to growth, samples were annealed at the growth temperature of 850 °C (thermocouple temperature) followed by a 10-minute oxygen plasma exposure using a radiofrequency (RF) plasma source with an oxygen BEP of ~ 1.0×10^{-5} Torr. In addition to a series of films grown without any co-supplied oxidant ("no oxygen" films), two additional series were grown using either molecular oxygen or oxygen RF-plasma, respectively. For the samples grown with oxygen plasma, growth proceeded directly following the 10-minute plasma anneal, keeping the same conditions for the plasma. The oxygen BEP was ~ 1.0×10^{-5} Torr during growth of films using molecular oxygen. For the samples grown without any co-supplied oxidant the chamber was allowed to pump for 5 minutes reduce background oxygen, followed by growth using only the Ba, La, and SnO_2 sources. For each condition, a series of films were grown at different SnO_2/Ba flux ratios to vary the cation stoichiometry. This was accomplished by holding the SnO_2 cell temperature constant and varying the Ba flux. This avoids changing the SnO_2 cell temperature as this will affect the partial pressures of the species evaporating from the SnO_2 source [23-25]. Growth times were adjusted to compensate for the change in growth rate with Ba flux to achieve film thicknesses ≥ 35 nm, which is sufficiently thick to achieve mobilities in the range of 150 $cm^2\ V^{-1}s^{-1}$ [11]. The growth rate was found to be Ba-limited for all films (Fig. 1). For each sample, an unintentionally-doped (UID) $BaSnO_3$ buffer layer was grown first, followed by the La-doped active layer. The UID buffer layer was grown using the same conditions as the active layer for 50% of the growth time.

We have found from previous studies that this thin buffer layer scheme is sufficient for achieving high mobility films and that the precise thickness of the buffer layer in this regime is negligible.

The La flux was adjusted to keep the doping density within the ~ 1×10^{19} - 3×10^{20} cm^{-3} range, in which mobility is relatively independent of the carrier density. It is important to note that the mobile carrier density is affected by the growth parameters that were varied in these experiments, not just the La flux. These include cation flux ratios and oxygen supply, which determine dopant activation and the concentration of compensating defects [22, 26], and the growth rate. In addition, effects from sample nonuniformity as well as variability in the electrical properties between samples grown under nominal identical growth conditions is a general issue for state-of-the-art $BaSnO_3$ films, as is also seen in the literature [12]. For this reason, differences in mobility values of a few 10's of $cm^2\ V^{-1}s^{-1}$ are not taken as significant for the purpose of this growth study, which focuses on systematic trends. We only use relative robust indicators in the electrical properties, such as insulating behavior and large deviations from high-mobility – which we will define as $\mu > 120\ cm^2\ V^{-1}s^{-1}$ – within this doping range as being indicative of the introduction of defects.

Reflection high energy electron diffraction (RHEED) was used to monitor the growth. Structural characterization was performed via high resolution x-ray diffraction (XRD): out-of-plane lattice parameters (a_{op}) were measured in a triple-axis configuration and film perfection was assessed using open detector scans. Straight-beam alignments were performed prior to every measurement to eliminate any residual instrument offset. All films were found to be relaxed (see Supplementary Information [27]). Film thicknesses were calculated from x-ray reflectivity (XRR) data. For films with poor XRR due to surface morphology (see Supplementary Information for atomic force microscopy of the film surfaces [27]), the thickness

was estimated from the Ba-flux, as the growth rate is Ba-limited (Fig. 1). For electrical measurements, Ti/Au ohmic contacts were deposited in van der Pauw geometry via electron beam evaporation. Sheet carrier densities and Hall mobilities were determined at room temperature using a LakeShore Hall Measurement System. To determine the reliability of the van der Pauw measurements, smaller Hall bar structures were fabricated from selected samples, which provide a measure of the variability in the mobility data due to film nonuniformity [27].

III. Results

Figure 2 shows XRD data of films grown with different SnO_2/Ba flux ratios, without any co-supplied oxidant, with molecular oxygen, and with oxygen RF-plasma, respectively. All films exhibit the 002 $BaSnO_3$ reflection, indicating successful epitaxial growth of the $BaSnO_3$ perovskite phase for all growth conditions. The no-oxygen sample grown at SnO_2/Ba = 15 also exhibits a wide hump on the low-angle side of the 002 $BaSnO_3$ peak, which can be seen more clearly in the wide-angle scans (not shown). This peak may belong to a Ba-rich phase, possibly Ruddlesden-Popper Ba_2SnO_4 [28]. Films grown with oxygen do not exhibit Ba-rich peaks in XRD. Some films also exhibit weak SnO_2 peaks in wide-angle scans.

X-ray rocking curves are shown in Figs. 2(d-f). Their widths represent the crystal surface quality and crystal perfection of the films' interiors. For example, for the films grown without additional oxygen [Fig. 2(d)], the narrow curves are also those that exhibit thickness oscillations in Fig. 2(a), indicating smooth surfaces. These films are grown with the highest SnO_2/Ba flux ratios and all have similar full width at half maxima (FWHM) values of 0.097°, 0.068°, and 0.099°. They differ, however, in the width of the lower portion of the rocking curve, which

typically contains the diffuse scattering from point defects. As shown in Fig. 2, the width the rocking curve wing correlates with the measured mobility, indicating that the point defects giving rise the intensity in this portion of the rocking curve are also the ones that affect the mobility.

Samples grown with additional oxidant show a less systematic relationship between carrier mobility and rocking curve widths. Oxygen tends to reduce the mobility of arriving adatoms species on the growing films surface [29]. This negatively affects crystalline perfection and surface quality and both cause broadening of the rocking curves. In addition, for some samples, the 220 peak from the $DyScO_3$ substrate displays a shoulder that is reflected in an asymmetry in the film rocking curve, such as for the 35.4 ratio film [Figs. 2(c) and 2(f)].

Figure 3 compares the measured out-of-plane lattice parameters (a_{op}) and Hall mobilities (μ). Note that samples that were too resistive to reliably measure the Hall mobility are displayed as having $\mu = 0$ $cm^2V^{-1}s^{-1}$. Three important observations can be made: (*i*) most measured a_{op} are smaller than the reported stoichiometric value for $BaSnO_3$ (indicated by the dotted line), (*ii*) the mobilities are highest near the minimum in a_{op}, rather than near the apparent stoichiometric value, and (iii) addition of oxygen shifts the growth conditions to achieve films that exhibit the highest mobility to lower SnO_2/Ba ratios, compared with films grown with no additional oxygen. In addition, slightly higher mobilities are achieved in the films grown with extra oxygen. We note that the small a_{op} is not caused by residual epitaxial coherency strains, as compressively strained films would lead to an expanded a_{op}.

IV. Discussion

A main result is the successful growth of $BaSnO_3$ without any co-supplied oxidant. This shows that oxygen-containing species needed to form the $BaSnO_3$ perovskite phase are mainly supplied by the flux from the SnO_2 cell. The main evaporating species from an SnO_2 source in a vacuum environment is SnO [23-25, 30]. Mass spectrometric studies indicate that the flux from SnO_2 at 1420 K contains approximately 77% SnO, 21% O_2, 1.5% Sn_2O_2, with the rest belonging to SnO_2 and other molecules [30]. The small amount of O_2 in the flux from a SnO_2 cell suggests that films grown without an additional oxidant are grown in oxygen-poor conditions. If SnO is the main source of oxygen, then growth conditions are likely also Sn-rich. Sn-rich conditions are supported by the fact that growth rate remains Ba-limited for most films (Fig. 1). In the absence of a true MBE growth window or for compounds that are not true line compounds, non-stoichiometric growth conditions will induce native point defects, such as vacancies or antisite defects [31-33].

We next discuss possible defects, beginning with the films grown with no additional oxygen. The deviation of the lattice parameter from its stoichiometric value provides information about the prominent defect(s). Cation vacancies cause a lattice expansion in most perovskites and may in $BaSnO_3$ as well [16, 34]. Oxygen vacancies cause virtually no variation in the lattice parameter of $SrTiO_3$ thin films [35], although there are indications that they may cause a moderate lattice expansion in $BaSnO_3$ [36]. In contrast, Sn^{2+} incorporation on the Ba-site may lead to a lattice contraction [17], because the Ba-site is large compared to the ionic radius of Sn^{2+}. In general, perovskites that incorporate Sn on the A-site are found to exhibit reduced lattice parameters [21, 37, 38]. Therefore, we posit that the small a_{op} are a fingerprint of Sn_{Ba} formation in these films. Given oxygen-poor, Sn-rich conditions, Sn_{Ba} is a likely

mechanism to accommodate Sn excess in the high-mobility films. This is also consistent with DFT calculations for these conditions [22, 26, 39].

On the low SnO_2/Ba flux ratio side, some films appear to possess a_{op} values that are closer to the stoichiometric values, though their poor electrical properties indicate that these films are not stoichiometric. A more likely scenario for the apparent stoichiometric a_{op} is another defect, which causes a lattice expansion compensates for the lattice contraction caused by Sn_{Ba}. According to DFT [22, 26], under Sn-rich conditions, Ba-vacancies ($V_{Ba}^{''}$) and Sn_{Ba} are favorable. Donor dopants may under certain conditions also favor cation vacancies [40]. In contrast to Sn_{Ba}, $V_{Ba}^{''}$ are likely to cause a lattice expansion and furthermore to act as acceptors [39]. From the change in lattice parameter seen in Fig. 3(a), it is apparent that $V_{Ba}^{''}$ are more favorable under conditions that are less Sn-rich and possibly also more oxygen poor (larger lattice parameter). As the SnO_2/Ba flux ratio is increased their concentration decreases, most likely by incorporation of Sn^{2+} on the empty Ba-sites, which causes the lattice parameter to decrease. The increase in mobility with increasing SnO_2/Ba flux can then be explained with Sn_{Ba} filling the negatively charged $V_{Ba}^{''}$, which should scatter more strongly by ionized impurity scattering and/or trap mobile carriers than the charge-neutral Sn_{Ba}. Ultimately, however, even charge-neutral defects contribute to carrier the scattering and reduce the mobilities. We note that another defect candidate causing a lattice expansion could be oxygen vacancies, $V_O^{\circ\circ}$. The high degree of La-doping should, however, suppress the formation of $V_O^{\circ\circ}$, while promoting compensating $V_{Ba}^{''}$ [26].

This general picture is further confirmed by considering the trends in the films grown with additional oxygen. Lower-than-stoichiometric a_{op} are exhibited by these films as well,

pointing to the presence of Sn_{Ba} defects. Therefore, it appears that even in the presence of additional oxygen during growth, even in the form of an activated plasma, the conditions are still Sn-rich. The main effect of additional oxygen supplied by the molecular or plasma source is to shift the growth conditions. The extra oxygen shifts the growth conditions for high mobility films toward lower SnO_2/Ba ratios. This is consistent with the interpretation discussed above: the extra oxygen alleviates the need to supply a large amount of oxygen via SnO, making the conditions less Sn-rich. Thus, the only way to improve the cation stoichiometry of $BaSnO_3$ films would be achieve vastly more oxidizing conditions, which appears to be difficult to achieve within the constraints of MBE. Already, one difficulty for the films grown with additional oxygen supply is the oxidation of the Ba source material and associated Ba flux instabilities [41].

Finally, we note that based on the observed variations in carrier density (n_{3D}), about ~1-4 $\times 10^{19}$ cm^{-3} for films grown at different cation flux ratios, the concentration of electrically active defects from non-stoichiometry is estimated to be less than 1%. This degree of nonstochiometry is difficult to detect with most thin film physical characterization methods, while nevertheless significant in terms of the electrical properties.

V. Conclusions

To summarize, we have demonstrated that La-doped $BaSnO_3$ films can be grown by MBE using only Ba, La, and SnO_2 effusion sources. Even when additional oxygen is supplied, however, lattice parameter measurements indicate that film are nonstoichiometric. We have argued that the films are Sn-rich and that the origin of this two-fold: SnO is a major source of the oxygen incorporated in the films and the dual valency of Sn facilitates the formation of Sn_{Ba}

antisite defects, which can accommodate Sn-excess. Moreover, the study showed that films with an apparent stoichiometric lattice parameter are, in fact, also nonstoichiometric, most likely because the effects of two defects on the lattice parameter compensate each other. Thus, unlike materials that are much closer to line compounds and can be fully oxidized, such as $SrTiO_3$, care should be taken to make claims of an MBE growth window based on lattice parameter measurements. In addition to developing substrates that have a reduced lattice mismatch, the key to achieve $BaSnO_3$ films with higher mobilities will be more oxidizing conditions, which is challenging in MBE.

Acknowledgements

The authors than Santosh Raghavan and Chris Freeze for many prior growth studies, reported in their Ph.D. theses, and many helpful discussions. The authors acknowledge funding by the Office of Naval Research (ONR) through Award No. N00014-18-1-2704 and the DARPA DREaM program (Award No. ONR N00014-18-1-2034). Preliminary studies were funded by the US National Science Foundation (Grant No. DMR-1409985). This work made use of the MRL Shared Experimental Facilities, which are supported by the MRSEC Program of the US National Science Foundation under Award No. DMR 1720256.

References

[1] H. J. Kim, U. Kim, H. M. Kim, T. H. Kim, H. S. Mun, B.-G. Jeon, K. T. Hong, W.-J. Lee, C. Ju, Kee Hoon Kim, and K. Char, Appl. Phys. Expr. **5**, 061102 (2012).

[2] H. J. Kim, U. Kim, T. H. Kim, J. Kim, H. M. Kim, B. G. Jeon, W. J. Lee, H. S. Mun, K. T. Hong, J. Yu, K. Char, and K. H. Kim, Phys. Rev. B **86**, 165205 (2012).

[3] X. Luo, Y. S. Oh, A. Sirenko, P. Gao, T. A. Tyson, K. Char, and S. W. Cheong, Appl. Phys. Lett. **100**, 172112 (2012).

[4] S. Ismail-Beigi, F. J. Walker, S. W. Cheong, K. M. Rabe, and C. H. Ahn, APL Mater. **3**, 062510 (2015).

[5] Z. B. Xia, C. Y. Wang, N. K. Kalarickal, S. Stemmer, and S. Rajan, IEEE Trans. Electron Devices **66**, 896 (2019).

[6] H. Chandrasekar, J. N. Cheng, T. S. Wang, Z. B. Xia, N. G. Combs, C. R. Freeze, P. B. Marshall, J. McGlone, A. Arehart, S. Ringel, A. Janotti, S. Stemmer, W. Lu, and S. Rajan, Appl. Phys. Lett. **115**, 092102 (2019).

[7] D. J. Singh, D. A. Papaconstantopoulos, J. P. Julien, and F. Cyrot-Lackmann, Phys. Rev. B **44**, 9519 (1991).

[8] H. Mizoguchi, P. M. Woodward, C. H. Park, and D. A. Keszler, J. Amer. Chem. Soc. **126**, 9796 (2004).

[9] T. Schumann, S. Raghavan, K. Ahadi, H. Kim, and S. Stemmer, J. Vac. Sci. Technol. A **34**, 050601 (2016).

[10] S. J. Allen, S. Raghavan, T. Schumann, K. M. Law, and S. Stemmer, Appl. Phys. Lett. **108**, 252107 (2016).

[11] S. Raghavan, T. Schumann, H. Kim, J. Y. Zhang, T. A. Cain, and S. Stemmer, APL Mater. **4**, 016106 (2016).

[12] H. Paik, Z. Chen, E. Lochocki, H. A. Seidner, A. Verma, N. Tanen, J. Park, M. Uchida, S. L. Shang, B. C. Zhou, M. Brutzam, R. Uecker, Z. K. Liu, D. Jena, K. M. Shen, D. A. Muller, and D. G. Schlom, APL Mater. **5**, 116107 (2017).

[13] M. Y. Tsai, M. E. White, and J. S. Speck, J. Appl. Phys. **106**, 024911 (2009).

[14] M. E. White, M. Y. Tsai, F. Wu, and J. S. Speck, J. Vac. Sci. & Technol. A **26**, 1300 (2008).

[15] Z. Lebens-Higgins, D. O. Scanlon, H. Paik, S. Sallis, Y. Nie, M. Uchida, N. F. Quackenbush, M. J. Wahila, G. E. Sterbinsky, D. A. Arena, J. C. Woicik, D. G. Schlom, and L. F. J. Piper, Phys. Rev. Lett. **116**, 027602 (2016).

[16] A. Prakash, J. Dewey, H. Yun, J. S. Jeong, K. A. Mkhoyan, and B. Jalan, J. Vac. Sci. & Technol. A **33**, 060608 (2015).

[17] A. Prakash, P. Xu, X. W. Wu, G. Haugstad, X. J. Wang, and B. Jalan, J. Mater. Chem. C **5**, 5730 (2017).

[18] E. H. Mountstevens, J. P. Attfield, and S. A. T. Redfern, J. Phys. Cond. Mat. **15**, 8315 (2003).

[19] A. K. Prodjosantoso, Q. D. Zhou, and B. J. Kennedy, J. Solid State Chem. **200**, 241 (2013).

[20] M. Batzill, and U. Diebold, Prog. Surf. Sci. **79**, 47 (2005).

[21] T. Q. Wang, K. C. Pitike, Y. K. Yuan, S. M. Nakhmanson, V. Gopalan, and B. Jalan, APL Mater. **4**, 126111 (2016).

[22] D. O. Scanlon, Phys. Rev. B **87**, 161201(R) (2013).

[23] R. H. Lamoreaux, D. L. Hildenbrand, and L. Brewer, J. Phys. Chem. Ref. Data **16**, 419 (1987).

[24] R. Colin, J. Drowart, and G. Verhaegen, Trans. Faraday Soc. **61**, 1364 (1965).

[25] E. Zimmermann, S. Königs, and D. Neuschütz, Z. Physikal. Chem. **209**, 271 (1999).

[26] L. Weston, L. Bjaalie, K. Krishnaswamy, and C. G. Van de Walle, Phys. Rev. B **97**, 054112 (2018).

[27] See Supporting Information [link to be inserted by publisher] for a representative reciprocal space map, atomic force microscopy images of the films surfaces, and mobility measurements using Hall bar structures.

[28] U. Kumar, and S. Upadhyay, J. Electron. Mater. **48**, 5279 (2019).

[29] E. J. Tarsa, E. A. Hachfeld, F. T. Quinlan, J. S. Speck, and M. Eddy, Appl. Phys. Lett. **68**, 490 (1995).

[30] E. K. Kazenas, M. A. Bol'shikh, and A. A. Petrov, Russian Metallurgy (Metally) **3**, 23 (1996).

[31] C. D. Theis, J.Yeh, D. G. Schlom, M. E. Hawley, and G. W. Brown, Thin Solid Films **325**, 107 (1998).

[32] D. G. Schlom, J. H. Haeni, J. Lettieri, C. D. Theis, W. Tian, J. C. Jiang, and X. Q. Pan, Mater. Sci. Eng. B-Solid State Mater. Adv. Technol. **87**, 282 (2001).

[33] J. Y. Tsao, *Materials Fundamentals of Molecular Beam Epitaxy* (Academic Press, Boston, 1993).

[34] B. Jalan, P. Moetakef, and S. Stemmer, Appl. Phys. Lett. **95**, 032906 (2009).

[35] T. Ohnishi, M. Lippmaa, T. Yamamoto, S. Meguro, and H. Koinuma, Appl. Phys. Lett. **87**, 241919 (2005).

[36] K. Ganguly, P. Ambwani, P. Xu, J. S. Jeong, K. A. Mkhoyan, C. Leighton, and B. Jalan, APL Mater. **3**, 062509 (2015).

[37] S. Suzuki, T. Takeda, A. Ando, T. Oyama, N. Wada, H. Niimi, and H. Takagi, Jpn. J. Appl. Phys. **49**, 09MC04 (2010).

[38] S. Suzuki, T. Takeda, A. Ando, and H. Takagi, Appl. Phys. Lett. **96**, 132903 (2010).

[39] S. KC, A. J. E. Rowberg, L. Weston, and C. G. V. d. Walle, J. Appl. Phys. **126**, 195701 (2019).

[40] Y.-M. Chiang, D. P. Birnie, and W. D. Kingery, *Physical Ceramics: Principles for Ceramic Science and Engineering* (John Wiley & Sons, 1997).

[41] E. S. Hellman, and E. H. Hartford, J. Vac. Sci. Technol. B **12**, 1178 (1994).

Figure Captions

Figure 1: Film growth rates as a function of Ba flux.

Figure 2: (a-c) On-axis 2θ-ω scans around the $BaSnO_3$ 002 reflection for films grown with (a) no additional oxygen, (b) molecular oxygen, and (c) oxygen plasma. (d-f) Rocking curves around the $BaSnO_3$ 002 reflection for films grown with (a) no additional oxygen, (b) molecular oxygen, and (c) oxygen plasma. The triangles mark the 002 $BaSnO_3$ film reflections and the asterixis mark the 220 $DyScO_3$ reflections.

Figure 3: Out-of-plane lattice constants a_{op} (orange circles, left axis) and measured Hall mobilities (blue triangles, right axis) as a function of SnO_2/Ba BEP ratio for films grown with (a) no additional oxygen, (b) molecular oxygen, and (c) oxygen plasma.

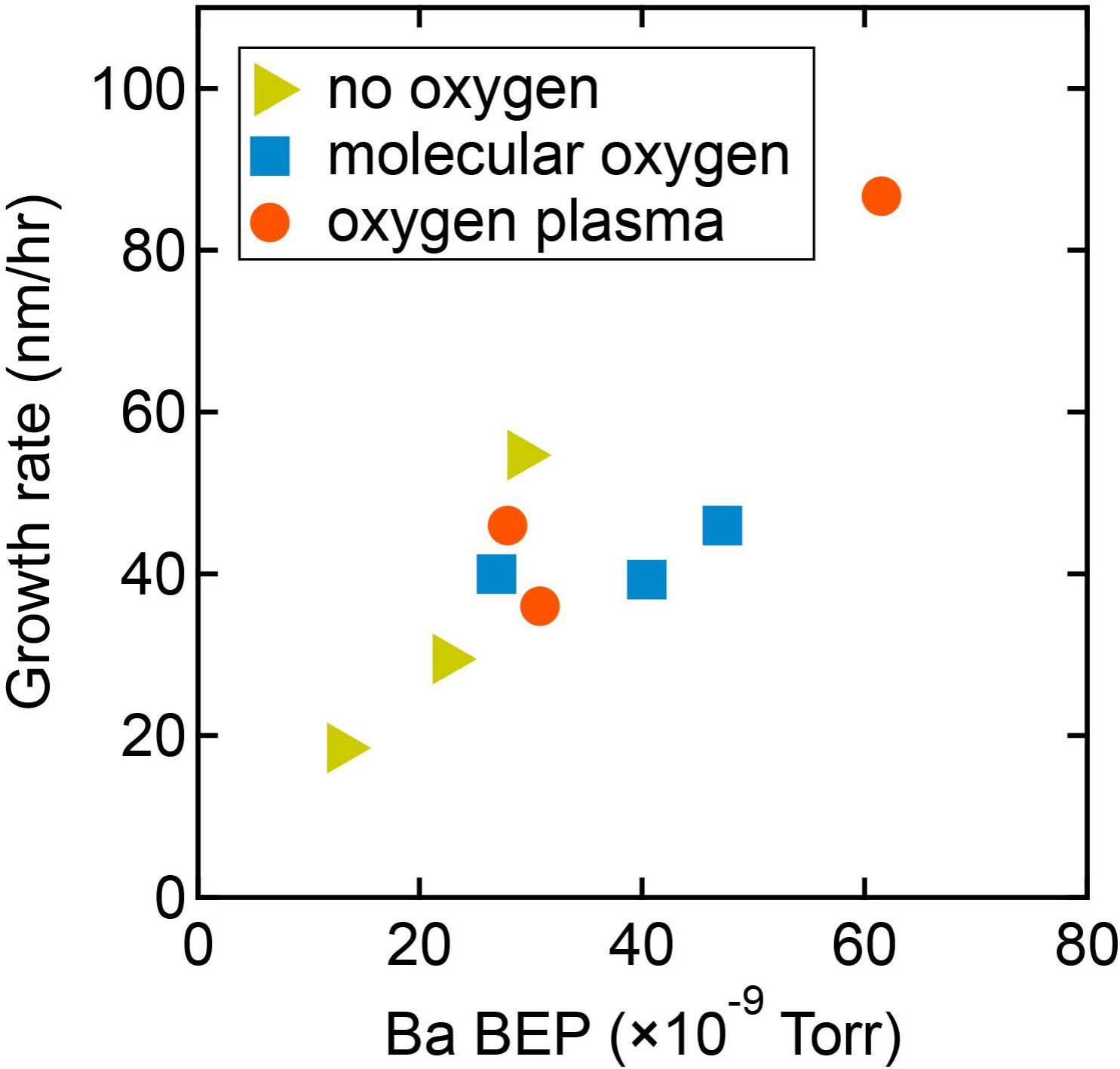
no oxygen
molecular oxygen
oxygen plasma
Growth rate (nm/hr)
0
20
40
60
80
100
0
20
40
60
80
Ba BEP (×10-9 Torr)

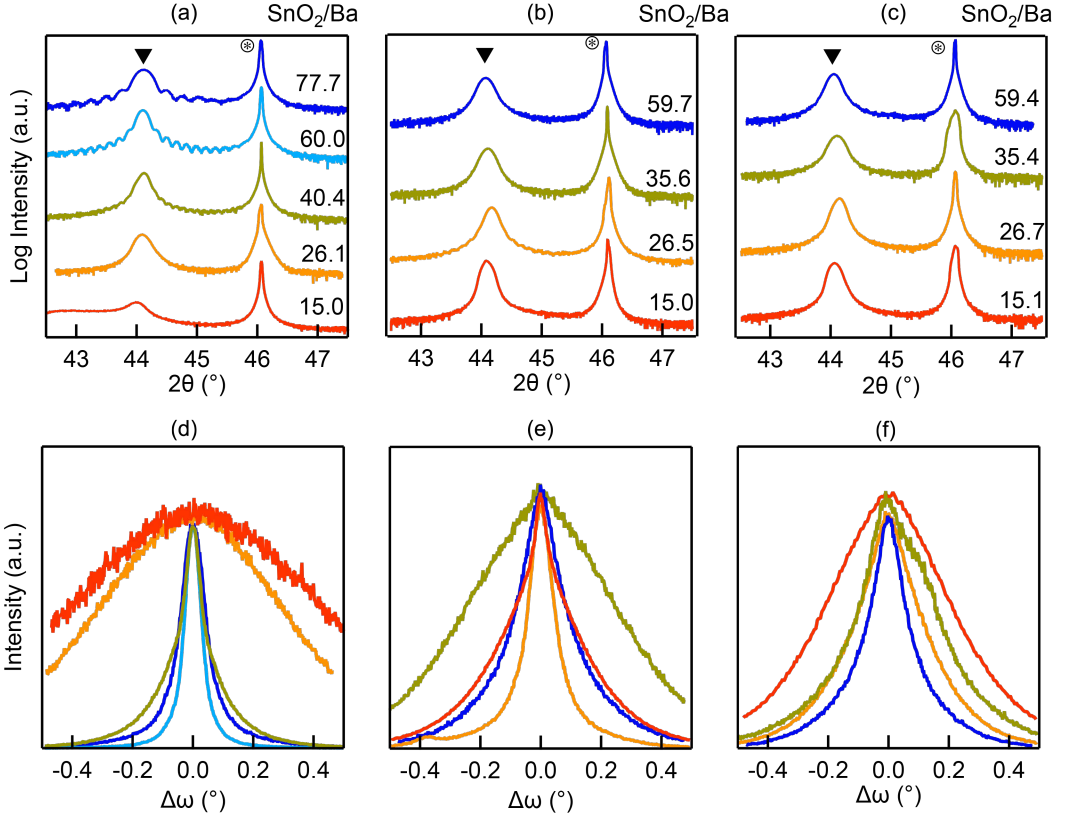
(a)
SnO2/Ba
77.7
60.0
40.4
26.1
15.0
Log Intensity (a.u.)
43
44
45
46
47
2θ (°)
(b)
SnO2/Ba
59.7
35.6
26.5
15.0
43
44
45
46
47
2θ (°)
(c)
SnO2/Ba
59.4
35.4
26.7
15.1
43
44
45
46
47
2θ (°)
(d)
Intensity (a.u.)
-0.4
-0.2
0.0
0.2
0.4
Δω (°)
(e)
-0.4
-0.2
0.0
0.2
0.4
Δω (°)
(f)
-0.4
-0.2
0.0
0.2
0.4
Δω (°)

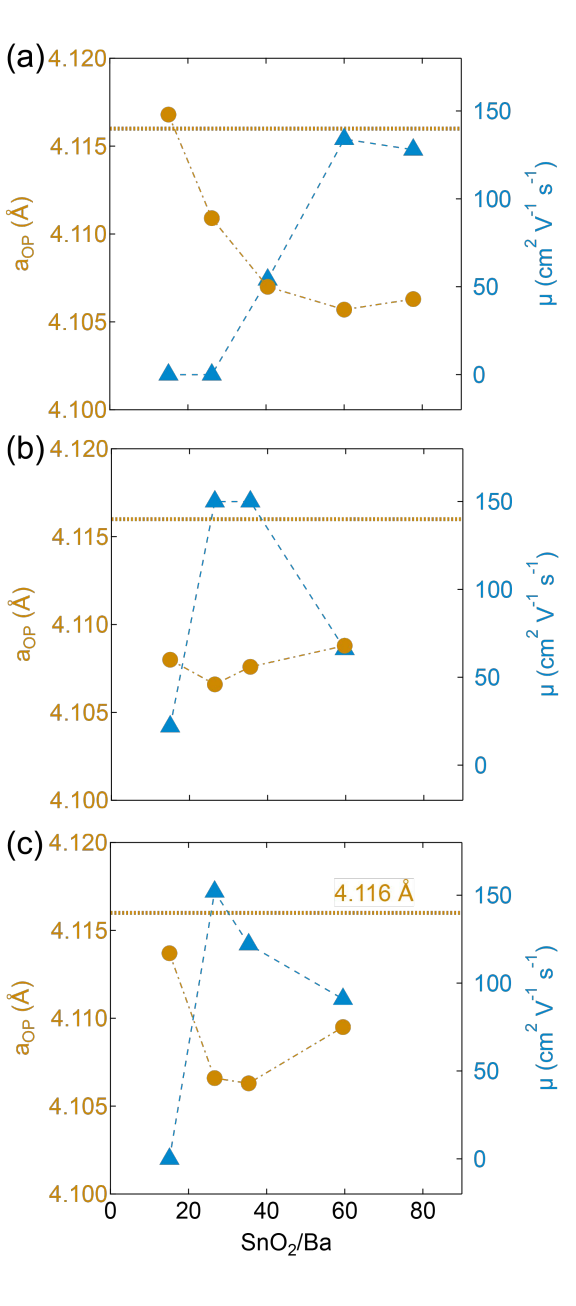
(a)
(b)
(c)
4.120
4.115
4.110
4.105
4.100
a_{OP} (Å)
150
100
50
0
μ (cm^2 V^{-1} s^{-1})
4.116 Å
0
20
40
60
80
SnO_2/Ba